Observed and modelled cloud cover up to 6 km height at Station Nord in the high Arctic

Gryning, Sven-Erik; Batchvarova, Ekaterina; Floors, Rogier Ralph; Münkel, Christoph; Skov, Henrik; Sørensen, Lise Lotte

Published in:
International Journal of Climatology

Link to article, DOI:
10.1002/joc.6894

Publication date:
2021

Document Version
Publisher's PDF, also known as Version of record

Received: 22 July 2020 | Revised: 3 October 2020 | Accepted: 13 October 2020

DOI: 10.1002/joc.6894

RESEARCH ARTICLE

International Journal of Climatology RMetS

Observed and modelled cloud cover up to 6 km height at Station Nord in the high Arctic

Sven-Erik Gryning[1] | Ekaterina Batchvarova[1,2] | Rogier Floors[1] | Christoph Münkel[3] | Henrik Skov[4] | Lise Lotte Sørensen[4]

[1]DTU Wind Energy, Technical University of Denmark, Roskilde, Denmark

[2]Climate, Atmosphere and Water Research Institute, Bulgarian Academy of Sciences (CAWRI-BAS), Sofia, Bulgaria

[3]Vaisala GmbH, Hamburg, Germany

[4]iClimate, Arctic Research Center, Department of Environmental Science, Aarhus University, Aarhus, Denmark

Correspondence
Sven-Erik Gryning, DTU Wind Energy, Technical University of Denmark, Roskilde, Denmark.
Email: sveg@dtu.dk

Funding information
European Cooperation in Science and Technology, Grant/Award Number: COST Action CA18235 PROBE; Monitoring of short lived climate components in Arctic in Danish: Monitering af kortlivede klimakomponenter i Arktis", The Danish Environmental Agency; National Science Fund of Bulgaria, Contract KP-06-N34/1 "Natural and anthropogenic factors of climate change - analyzes of global and local periodical components and long-term forecasts"., Grant/Award Number: KP-06-N34/1

Abstract

We present results from an analyses of cloud cover based on profiles of the attenuated backscatter coefficient from an 8-year-long data series (July 2011–April 2019). The observations are carried out in the high Arctic by a ceilometer with a maximum range setting of 7.7 km from the Villum Research Station at Station Nord, Greenland. Results show that the hourly cloud cover turned out to follow a U-shaped rather than Gaussian-like distribution. Annual and seasonal cloud cover variation is illustrated. The cloud cover is larger during the autumn and winter as compared to summer and spring. The cloud cover exhibits a substantial variation from year to year without a clear trend. The cloud cover during spring is low and decreasing between 2012 and 2017. The cloud cover during the autumn of 2016 is lowest compared to the other years. The observed cloud cover is compared to the cloud cover provided in the ERA5 reanalysis dataset. The cloud cover for low clouds and medium clouds are combined to represent a total height of 6 km. Both the observed and modelled cloud cover is larger during winter as compared to summer-time cloud cover. The measured reduction in the cloud cover for the autumn of 2016 is present in the reanalysis data as well but the measured low cloud cover during spring is not apparent in the reanalysis data. Because the cloud cover distribution is U-shaped rather than of a Gaussian nature, standard metrics are not applicable. We apply a generalized skill score that is developed for contingency tables or joint histograms. Three skill scores were calculated. It was found that for all three methods, skills for the predictability of the cloud cover by the ERA5 modelling is better for winter than summer and is poor during the spring.

KEYWORDS

ceilometer, cloud cover, ERA5, generalized skill score, high Arctic

1 | INTRODUCTION

Knowledge and understanding of Arctic cloud properties is important for climate predictions and weather forecasts but limited because of scarcity of observational data on Arctic clouds in general and especially during the dark winter season. Prediction of clouds is known to be a major challenge in numerical weather forecasts and climate models (Karlsson and Svensson, 2011), and the shortage of observations for use in data-assimilation in the Arctic constitute a further challenge.

Aircraft measurements provide a detailed in situ view of the microphysical cloud properties and their relationship with atmospheric parameters but are limited to case studies and process-oriented study missions (Hobbs and Rangno, 1990; Curry *et al*., 1996; Pinto, 1998; McFarquhar *et al*., 2007; Suomi *et al*., 2016).

Satellites, although providing the greatest spatial and temporal cover, are unmatched with other platforms with near-global coverage but limited by polar-orbital tracks that rarely exceed 81°N. Furthermore, because of the state of the underlying snow/ice, surface there is little visible thermal or microwave contrast between the clouds and the highly reflective underlying surface, and standard threshold techniques are inadequate (Key and Barry, 1989; Rossow, 1993; Curry *et al*., 1996; Shupe *et al*., 2011; Chernokulsky and Mokhov, 2012).

Visual observations of clouds in the Arctic are not only sparse but, according to Hahn *et al*. (1995), they are also problematic during the dark winter season due to inadequate illumination of the clouds. Hahn *et al*. (1995) found dependence between the visual cloud classification during the night-time and the illumination of clouds by moonlight or twilight, in such a way that the average cloud cover at night is underestimated in cloud climatology based on visual observations.

When working with cloud climatology, it should be emphasized that a universally accepted definition of a cloud is lacking, even yet! In relation to climate research, for example, there can be emphasis on radiation and specific wavelengths. This is in contrast to solar energy where the whole spectrum of wavelengths contributes to the energy in the relevant parameter—summing up to the total incoming radiation. Cloud statistics are often studied using observations made by surface observers, or some minimum particle size in the cloud, or by the ability of a sensor to detect a signature in the cloud. Therefore, the understanding of what a cloud actually is depends entirely on the objectives of the study and the instrument and the observations that are used to estimate the clouds. Any cloud is therefore specific to the instruments that are used to observe it.

Long-term data series retrieved from ceilometers exist at several observatories, typically obtained with a variety of commercially available ceilometers and cloud detection algorithms. Older instruments were blind above 3,650 m and the continuous development of instruments did not only increase the height where the instrument became blind, but also improved software for cloud detection has increased the signal-to-noise ratio and thus the instruments ability to detect thin clouds. Overall, long-term datasets obtained by combining observations from ceilometers of different types and make are inhomogeneous regarding the detection of clouds and should be used cautiously for detection of long-term trends.

Long-term cloud observations in the Arctic have been carried out with remote sensing instruments in a sparsely distributed network stretching from Alaska over Canada to Svalbard (Norway; Shupe *et al*., 2011) and Tiksi (Siberia, Russia; Uttal *et al*., 2013). The network covers coastal locations with different climatic conditions from the predominantly ice-covered sea at Barrow that experience a decreasing amount of sea ice near the shore during the autumn, to Ny-Ålesund located in the Golf Stream at Svalbard and Tiksi eastward of Lena river estuary near the coast of the Laptev Sea. In addition, there is a number of observing stations with shorter time series—typically about 1 year—as Eureka in the Canadian archipelago and Summit on the Greenland inland ice. At these stations, clouds were observed by use of remote sensing techniques but with different instruments and software for cloud detection. Therefore, each of the stations provides a unique perspective of the clouds but comparison of the observations for the whole network is a challenge due to the different lengths of the observational time series and differences in remote sensing instruments. Furthermore, although in the cases where long-time series exist, for example, at Barrow (Alaska) and Ny-Ålesund (Svalbard, Norway) about 25 years of continuous measurements has been collected, there have been replacements of instruments and software, challenging the creating of long coherent time series and cloud statistics. Sometimes the corresponding operational proprietary software for the detection of cloud heights from the instrument producer is applied, in which cases the applied threshold values are not evident. As a consequence, the cloud classification statistics differs between the sites in the network, making it difficult to draw overarching conclusions for the entire network.

This study deals with the annual and seasonal variation of the cloud occurrence fraction observed at the Villum Research Station (VRS), at Station Nord in Northeastern Greenland. More than 8 years of observations (2011–2019) with a ceilometer and concurrent data of cloud cover from numerical reanalysis are applied. The

site and instruments are presented in section 2. A description of the reanalysis model (section 3) is followed by postprocessing of the measurements from the ceilometer and the numerical reanalysis data (section 4). Next is a description of the annual and seasonal variability of the cloud cover (section 5) and finally a presentation of the predictive ability of the numerical reanalysis data and various skill scores are introduced and discussed (section 6).

2 | SITE AND INSTRUMENTS

Station Nord is a military outpost on Princess Ingeborg Halvø in the Crown Prince's Christian Land, in Northeastern Greenland (81°36′N, 16°40′W; Figure 1). It is the northernmost permanently inhabited man-made location in Greenland only 924 km south of the geographic North Pole and 1,700 km north of the Polar circle. The nearest town is Longyearbyen on Svalbard (Norway), 720 km east of Station Nord, while the nearest town in Greenland is Ittoqqortoormiit, 1,250 km to the south. Further to the north are only the former Arctic research stations Brønlundhus and Kap Harald Moltke at Jørgen Brønlund Fjord in Pearyland. Station Nord can only be reached by plane as ice barriers block the sea. The dog sledge Sirius patrol, enforcing national sovereignty in North and Northeastern Greenland, uses Station Nord as a support and refurbishment base.

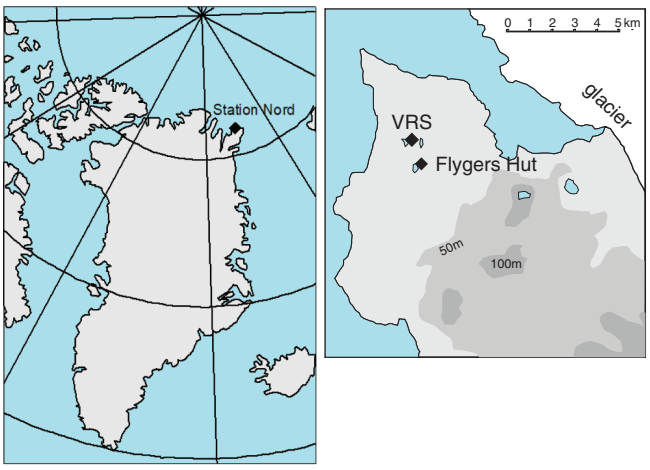

FIGURE 1 Maps showing in the left panel the location of Station Nord in Greenland and in the right panel the location of the VRS at Station Nord and surroundings of Flyger's Hut where the measurements were carried out. Blue is the open or frozen sea and lakes. On the left panel longitudes 120°W, 90°W, 60°W, 30°W, 0°, 30°E and 60°E and latitudes 80°N, 70°N and 60°N are indicated. In the right panel the elevation of the land is shown by grey scales [Colour figure can be viewed at wileyonlinelibrary.com]

The station is also used by researchers as a gateway for scientific expeditions to northeastern Greenland. Those expeditions are today centred on the VRS, which is a substantial upgrade of an existing air pollution monitoring station. The station hosts individual scientific projects focusing on atmospheric chemistry and physics. In addition to this, the station is used as a permanent base for an extensive long-term monitoring program with focus on atmospheric pollution and greenhouse gasses within the framework of the Arctic Monitoring and Assessment Programme (AMAP) (www.amap.no; Skov *et al*., 2017; 2020) and the Integrated Carbon Observation System (ICOS; www.icos-cp.eu).

The temperature is generally low; the climatologically warmest month is July with a mean temperature of 4°C; the winter is generally cold and below −20°C; the climatologically coldest month is March with an average temperature of −26°C. The enhanced warming in the Arctic (Boy *et al*., 2019), termed Arctic amplification, can also be observed at Station Nord.

The area is generally flat and snow covered most of the year. There are 100 m high hills a few km to the southeast and Flade Isblink glacier to the east. The thick permanent inland ice is more than 100 km away towards the southwest.

2.1 | Ceilometer

Measurements of backscatter profiles were carried out with a Vaisala CL51 diode laser ceilometer that was installed on the roof of the old monitoring hut—named Flyger's Hut—located 2.5 km south of the outpost (Figures 1 and 2).

A ceilometer is an active fully automatic 24/7 operational instrument that transmits very short (110 ns) pulses of light, vertically or near vertically, corresponding to an effective pulse length of about 16 m. The beam is backscattered as it impacts on aerosols and clouds. A new lidar pulse is emitted every 100 μs. The returned backscattered light is collected and converted to a digit every 67 ns, corresponding to a sampling rate of 15 MHz, which allows for a spatial resolution of 10 m. The first observation at 10 m represents the backscattered signal from 5 to 15 m. Laser pulses are emitted with a frequency of 10 kHz for about 1.6 s, after that an idle period of 0.4 s is used to run the firmware algorithm to process the data, followed by the emission of the next set of light pulses.

The instrument is operated on a wavelength of 905 nm with a beam divergence of about 0.4 mrad (milliradians) thus the probing area at a 1,000 m height is about 1 m^2. It is a single lens design which means that the observations reach complete optical overlap at low

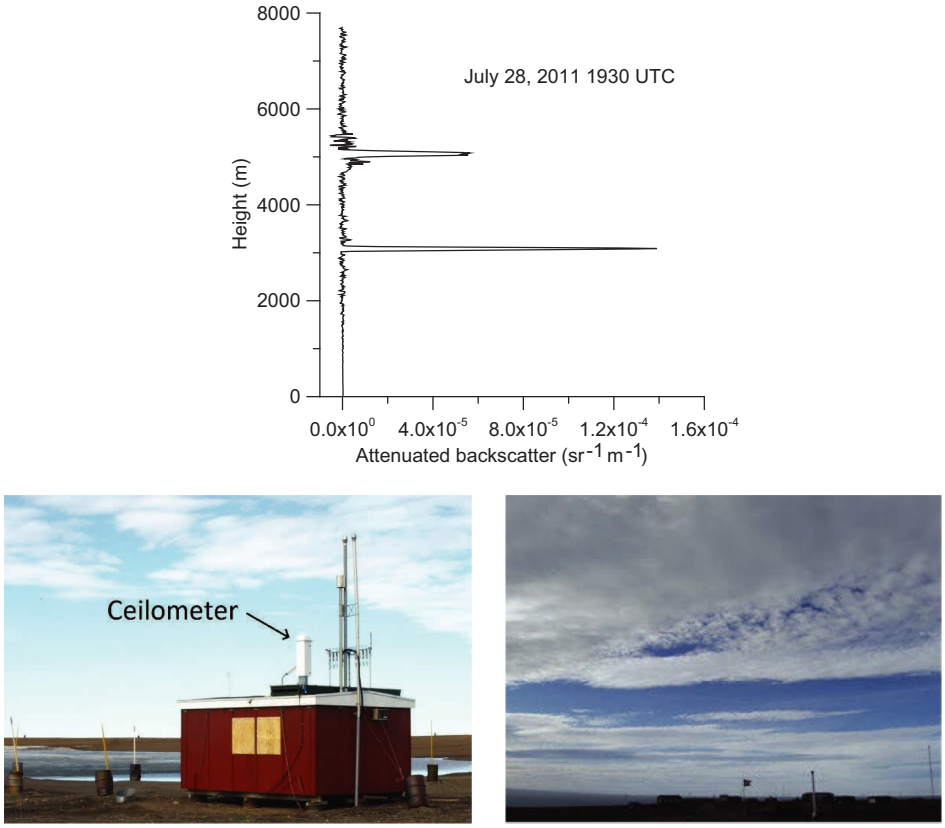

FIGURE 2 Example from July 28, 1930 UTC of a profile of the attenuated backscatter coefficient (upper panel) and a concurrent photo of the sky (lower right panel). Flyger's Hut with the ceilometer mounted on the roof is shown in lower left panel [Colour figure can be viewed at wileyonlinelibrary.com]

ranges, which are usable from the first or second range gate onwards. The range is taken as the distance from the instrument to the centre of the range gate. The backscatter signal is received by an avalanche photo diode (APD) detector and recorded. The backscatter of the laser pulses originating from aerosols and water vapour droplets in the air as well as raindrops, liquid and ice particles is detected by the ceilometer and is used in this study to identify the first cloud base layer.

From the start of the measurements on May 12, 2011 the ceilometer was operated with a resolution of 60 s and 10 m and a maximum range of 13,000 m. On March 20, 2013 the instrument was taken back for service and on that occasion the resolution changed to 16 s and 10 m and with a maximum range of 7,700 m. The instrument with the new settings was back in operation on August 22, 2013 and the analysis presented here covers data from then until April 12, 2019. The measurements are still ongoing (February 2020).

To secure proper performance and operation of the instrument, a number of internal checks are performed and the results are logged. Important parameters are

TABLE 1 Internal stability parameters logged as a part of the internal check of the ceilometer performance at Station Nord

Year	Laser energy as a percentage of nominal factory setting	Window transmission (%)	Temperature (°C)
2011	100.17	99.38	25.32
2012	100.05	99.95	25.30
2013	100.32	99.98	25.33
2014	100.08	99.83	25.43
2015	100.27	99.98	25.47
2016	100.27	99.97	25.54
2017	99.97	99.88	26.24
2018	100.11	99.86	25.40
2019	99.96	99.99	25.27

given in Table 1, suggesting that the ceilometer is performing well throughout the measuring period with respect to laser power, internal temperature and transmission through the lens. However, a drift in the sensitivity over the years cannot be excluded entirely.

3 | REANALYSIS MODEL OUTPUT

Model estimates of the cloud cover at Station Nord are obtained from reanalysis data. Reanalyses provide a numerical description of the recent climate by combining models with observations in a consistent way. Many reanalysis datasets have been developed. Here meteorological data from the ERA5 dataset is used (Hersbach *et al*., 2020), being the fifth major update developed by the European Centre of Medium-Range Weather Forecasts (ECMWF) as part of the Copernicus Climate Change Service (C3S) co-operation. ERA5 represents the latest adaption of the continuously improved reanalysis products in terms of grid size and temporal resolution as well as ingestion of improved interpretations of the original observations. ERA5 was produced using 4D-Var data assimilation in ECMWF's Integrated Forecast System (IFS). It is based on 18 hourly meteorological forecasts and analyses of the meteorological fields. It provides hourly estimates made possible using a 4D-Var assimilation method, even at locations where the observational coverage is sparse such as the high Arctic. It should be noted that unlike the IFS, the reanalysis output data are based on a static modelling system, which does not benefit from the continuous improvements and developments of the IFS modelling system. The version of the IFS modelling system that is used here is the CY41r2.

The ERA5 simulations are performed with 137 hybrid sigma/pressure (model) levels in the vertical, with the top level at 0.01 hPa which are interpolated to 37 pressure levels on a horizontal reduced-Gaussian grid with a spatial resolution of ≈31 km. Cloud fractions are derived at the model pressure levels from the simulated cloud liquid water, cloud ice, rain and snow. Details can be found in Forbes and Tompkins (2011), Forbes *et al*. (2011) and Forbes and Ahlgrimm (2014).

In this study, the cloud cover at each pressure model level is not applied but only the bulk cloud-cover data derived from the ERA5 simulations are used. The proportion of the bulk cloud cover in a grid box is given as hourly 2D single level variables for four altitudes, corresponding to the total, high, mid-level and low cloud cover. The bulk of the cloud cover values for each height range are calculated from the cloud cover at the model pressure levels using a generalized cloud overlap assumption in accordance with Hogan and Illingworth (2000) and Mace and Benson-Troth (2002). The low cloud cover is calculated from clouds that occur on model levels with a pressure greater than 0.8 times the surface pressure corresponding to a height of approximately 2 km. The medium cloud cover represents clouds at pressure levels between 0.45 and 0.8 times the surface pressure or approximately between 2 and 6 km in height, and high cloud cover represents clouds at pressure levels less than 0.45 times the surface pressure, or from approximately 6 km to the top of the atmosphere.

4 | POSTPROCESSING

4.1 | Reanalysis data of cloud cover

Here we aim at deriving the cloud cover for a height up to 6 km by combining the estimates of the cloud cover from the ERA5 up to 2 km, $C_{\mathrm{ERA5}}l$ and between 2 and 6 km, $C_{\mathrm{ERA5}}m$. As shown by Tompkins and Di Giuseppe (2015), the vertical overlap of cloudy layers separated by clear sky can be very erratic and depending on the type of cloud, it might even be site dependent. Use of different methods to estimate the way that clouds in different layers overlap in a grid box can have a considerable effect on the derived cloud cover for the entire layer. In order to derive the actual overlap in a vertical layer, several idealized methods (Hogan and Illingworth, 2000; Tompkins and Di Giuseppe, 2015) have been suggested, which will briefly be described here.

For a two-layer model it can be performed by assuming maximum overlap of the clouds in the two layers, $C_{\mathrm{ERA5}}\mathrm{max}$ which amounts to

$$C_{\mathrm{ERA5}}\mathrm{max} = \max(C_{\mathrm{ERA5}}l, C_{\mathrm{ERA5}}m), \quad (1)$$

which corresponds to the minimum possible cloud cover. Alternatively, by assuming a minimum possible overlap, $C_{\mathrm{ERA5}}\mathrm{min}$, becomes

$$C_{\mathrm{ERA5}}\mathrm{min} = \min(1, C_{\mathrm{ERA5}}l + C_{\mathrm{ERA5}}m), \quad (2)$$

corresponding to the maximum possible cloud cover. It should be noted that $C_{\mathrm{ERA5}}l + C_{\mathrm{ERA5}}m$ can be larger than one. Both expressions represent extreme and very unlikely cases. It is evident that the cloud cover can be anywhere between these extreme cases. A more realistic approach is to combine the cloud cover in the two layers by assuming random overlap, $C_{\mathrm{ERA5}}\mathrm{rand}$, is described in Hogan and Illingworth (2000) and Tompkins and Di Giuseppe (2015), which corresponds to

$$C_{\mathrm{ERA5}}\mathrm{rand} = C_{\mathrm{ERA5}}l + C_{\mathrm{ERA5}}m - C_{\mathrm{ERA5}}l\,C_{\mathrm{ERA5}}m. \quad (3)$$

Based on observations from a cloud radar in the United Kingdom, Hogan and Illingworth (2000) developed an alternative overlap approach, $C_{\mathrm{mea}}\mathrm{HI}$ using a combination of $C_{\mathrm{ERA5}}\mathrm{max}$ and $C_{\mathrm{ERA5}}\mathrm{rand}$,

$$C_{\mathrm{mea}}\mathrm{HI} = \alpha C_{\mathrm{ERA5}}\mathrm{max} + (1-\alpha)C_{\mathrm{ERA5}}\mathrm{rand}. \quad (4)$$

In the case described in Hogan and Illingworth (2000) the overlap parameter, α, was determined entirely from time series of cloud cover derived from cloud radar observations.

The last option, Equation (4) is implemented in this study. When applying the cloud cover that is measured by the ceilometer up to a height of 6 km (corresponding to the top of the medium high clouds in ERA5) and the cloud cover from the ERA5 simulations for the entire length of the time series of the ceilometer, the best fit for the overlap parameter, α, is found to be 0.8.

4.2 | Cloud detection by the ceilometer observations

There exists a large variety of ways to define a cloud in terms of a remote sensing signal (Vande Hey, 2015). In this study the attenuated backscatter coefficient profile from the ceilometer at Flyger's Hut at Station Nord is used to determine the cloud cover quantities. A ceilometer most reliably detects the presence of the first (lowest) cloud layer and because only statistics on the occurrence of the lowest clouds are needed for the analysis, there is no need to consider if there are any more clouds above the first cloud layer. Here the lowest 90 m is excluded in order to minimize the effect of fog and shallow blowing snow layers.

A cloud is detected when the threshold in the attenuated backscatter profile exceeds a predetermined threshold value. Commonly, for example, Platt *et al*. (1994), the threshold value is scaled with the standard deviation of the background signal in the attenuated backscatter profile. Since the background signal and its standard deviation are extremely small in the clear Arctic air, it is troublesome to apply common methods that are based on the standard deviation in the pristine Arctic air. Therefore, a simpler method that overcomes this special problem for the Arctic air is applied here. A cloud is assigned when a bin in the profile of the attenuated backscatter exceeds a prescribed threshold value. The attenuated backscatter profile must exceed the threshold value for a given number of adjacent height levels (bins) in order to be a candidate for a cloud. The latter ensures a certain robustness in the cloud detection algorithm. The analysis was performed with one, two and three bins and the results were found not to be sensitive to the selected number of bins.

Illingworth *et al*. (2007) suggested a threshold value of 2×10^{-5} sr^{-1} m^{-1} for detection of the liquid cloud base (the so-called Cloudnet approach). This is also the value used by Tuononen *et al*. (2019) in a study of clouds over Helsinki, Finland. Backscatter coefficients for a given cloud type is suggested by Vaughan (2002) for the visible and near-infrared regime and thus applicable for a ceilometer, although it is acknowledged that these values are uncertain and only appropriate when there is a very clear boundary layer below the clouds—as is often the case for the air in the Arctic. A value of 1.4×10^{-5} sr^{-1} m^{-1} was assigned to cirrus clouds in the classification by Vaughan (2002). Here threshold values of 10^{-5} sr^{-1} m^{-1} and 2×10^{-5} sr^{-1} m^{-1} were applied and the results were found not to be sensitive to the choice of the two threshold values. It was consequently decided for this study to use a threshold value of 2×10^{-5} sr^{-1} m^{-1}. It can be noted that the use of this threshold value for the attenuated backscatter coefficient agrees well with the cloud cover that is retrieved by the proprietary operational software from Vaisala that is used to identify the height at which the pilot can usually see the ground well.

Therefore in this study, a threshold value of 2×10^{-5} sr^{-1} m^{-1} that exceeds two consecutive levels in the profile of the attenuated backscatter is applied for cloud detection.

5 | SEASONAL AND ANNUAL VARIABILITY OF CLOUD COVER

5.1 | Definition of seasons

The analysis of the data will be presented in terms of seasonal variability and trends over whole years. The traditional definition of the seasons is not relevant in the high Arctic due to the extensive periods of midnight sun and days where the sun is below the horizon all the time. Here the seasons are defined according to the sun's position relative to the horizon (Table 2). Winter is considered as the period when all parts of the sun are below the horizon all of the time, and summer when some parts or all of the sun is above the horizon all the day. Defining the seasons in this way, the winter becomes shorter than the summer by about 16 days. Spring and autumn are equally long, corresponding to periods of daily changing between day and night. Other definitions are possible that take into account the twilight. When the sun sinks more than 18° below the horizon complete and

Season	Definition	Start-end	Number of days
Winter	Sun down all day	October 17–February 24	131
Spring	Day and night	February 25–April 9	44
Summer	Sun up all day	April 10–September 3	147
Autumn	Day and night	September 4–October 16	43

TABLE 2 Definitions of the seasons used in the study

Note: The periods are specific for the latitude of Station Nord. Sun down all day refers to the period when the sun is below the horizon all the time. For sun up all day the whole sun or part of it is visible all the time.

permanent darkness without twilight prevails. Even as far north as Station Nord, the sun is never below 18° at midday. Therefore there will always be periods of twilight during the Polar night.

5.2 | Averaging

The cloud cover that can be determined from numerical model output is fundamentally different from the cloud cover derived from observations by a ceilometer or any ground based remote sensing instrument. In the context of numerical modelling, cloud cover is defined as the fraction of a model grid that contains clouds at a given time, and in the context of ceilometer observations it is taken as the time clouds are observed by a zenith-pointing ceilometer.

To make a connection between the modelled and observed cloud cover, it is assumed that the time it takes for a cloud to be advected through a grid box corresponds to the time that the ceilometer observations are averaged.

In the ERA5 dataset the grid has a spatial resolution of ≈31 km. Typically in the literature a 1-hr averaging time is used which in this case corresponds to an advection wind speed of ≈9 m s^{-1}. For simplicity a 1-hr averaging time for the observations of cloud cover by the

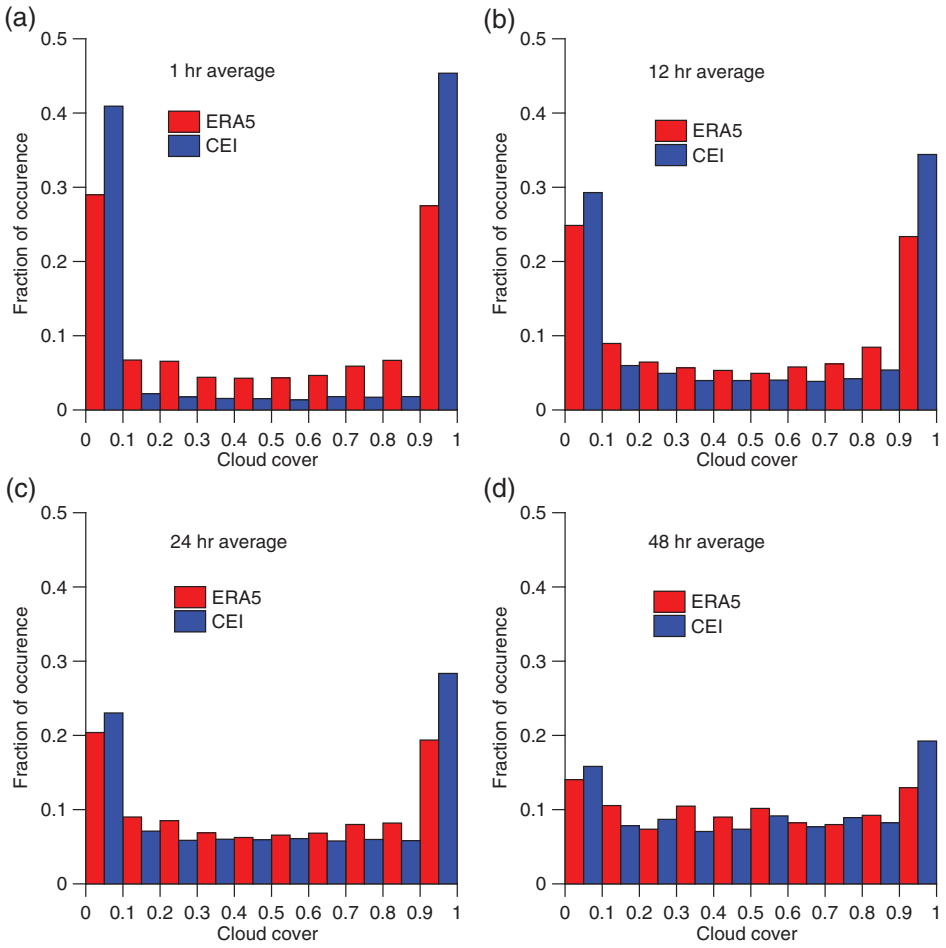

FIGURE 3 Histogram of the cloud cover of ceilometer observations (CEI) and derived from the reanalysis data (ERA5) up to a height of 6 km for the total period of measurements. (a–d) represent averaging times of 1, 12, 24 and 48 hr, respectively [Colour figure can be viewed at wileyonlinelibrary.com]

ceilometer will be applied here, which also corresponds to the time between the values of the instantaneous cloud cover that are provided by the numerical model. However, the dependence on wind speed should be kept in mind when comparing cloud cover from the ERA5 numerical modelling with the ceilometer observations.

Figure 3a shows the histogram of the hourly cloud cover derived from both the ERA5 simulations as well as the ceilometer observations. It is characteristic that it does not resemble a Gaussian type distribution but it is U-shaped. This feature is found both for the ceilometer observations as well as the ERA5 simulations and in such a way that there are more observations from the ceilometer for both cloud free and overcast conditions compared with the ERA5 simulations. Consequently, there are fewer observations for broken cloud cover from the ceilometer than from the ERA5 simulations. This feature that the distribution is U-shaped is often found for cloud cover distributions originating from ceilometer and cloud radar measurements, for example, in England (Hogan *et al.*, 2001; Hogan *et al.*, 2009), Austria (Rau and Piringer, 2018) and Finland (Tuononen *et al.*, 2019).

The occurrence of low level Stratus (St) and Stratuscumulus (Sc) clouds, which are due to mainly advection, is a characteristic feature of the planetary boundary layer in the Arctic and occurrences of convective clouds such as Cumulus are rare (Esau and Sorokina, 2011). This result in a tendency in the Arctic to have more fully cloud covered conditions when clouds are present, and similarly more periods with a clear sky as compared to areas with a mix of advective and convective clouds which is typical for Europe (except for the most northern part). Therefore, the conditions for clouds in the Arctic differ from the conditions described in Hogan *et al.* (2001), Rau and Piringer (2018) and Tuononen *et al.* (2019). The Arctic will have a tendency to have more fully cloud cover or clear sky conditions—in agreement with the observations.

The sensitiveness to the averaging time for the cloud cover distribution is illustrated in Figures 3b–d. It can be seen that the histogram of the cloud cover levels out in

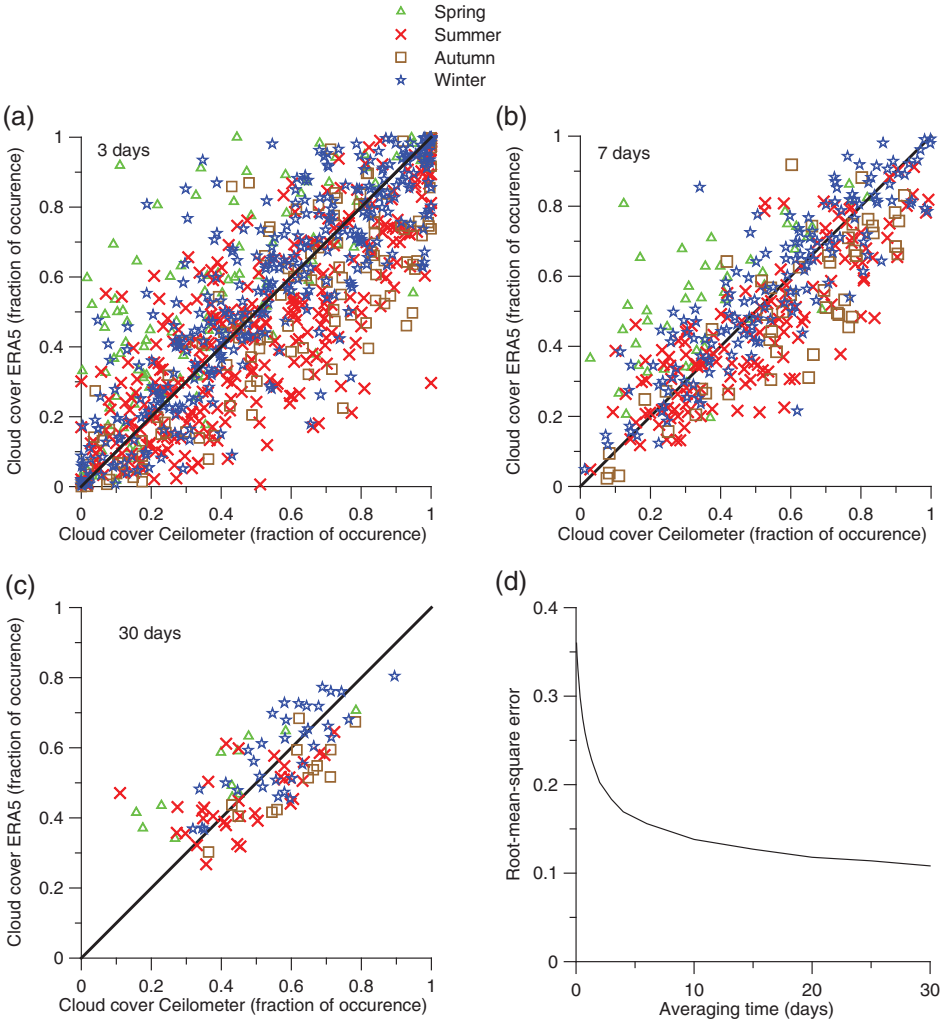

FIGURE 4 Scatter diagram of cloud cover derived from ceilometer observations versus reanalysis data for averaging times of 3, 7 and 30 days, as well as the root-mean-square error between observed and reanalysis data of the cloud cover as a function of the averaging time [Colour figure can be viewed at wileyonlinelibrary.com]

such a way that frequency of observations in the two extreme bins (0–0.1 and 0.9–1) decreases and the frequency in the bins between the two extremes increases for increasing averaging time.

In addition to the calculation of the distribution of the one-hourly ERA5 snapshots and the one-hourly averaged ceilometer observations, plots are presented in Figure 4 showing the overall scatter as well as seasonal behaviour of observed versus simulated cloud cover for an averaging time of 3, 7 and 30 days (Figure 4a–c). The agreement for spring and summer is better than autumn and winter. The root-mean-square error between observed and simulated cloud cover as a function of the averaging time is given in Figure 4d, which illustrates that the root-mean-square error decreases and thus the ability to predict the cloud cover improves with increasing averaging time. In other words, increasing the scale of the cloud-structures improves the skill to simulate the cloud cover. The annual cloud cover is illustrated in Figure 5 for all years with full datasets of observations.

5.3 | Seasonal and annual variability

Analysis of the average yearly and seasonal cloud cover derived from the ceilometer observations (Figure 6a) shows that the cloud cover exhibits a substantial variation both between seasons and from year to year. It can be seen that the cloud cover during spring (0.37 ± 0.005) and summer (0.51 ± 0.003) is lower in general than during autumn (0.59 ± 0.003) and winter (0.55 ± 0.003) where the number in brackets is the average and standard deviation of cloud cover over all the years in the analysis. There is variation in the averaged cloud cover from season to season and year to year. A clear trend in the seasonal and annual cloud cover cannot be observed, except for the spring where the cloud cover is persistently less than during the other seasons and decreases over time between 2012 and 2017. The absence of discernable trend during summer, autumn and winter periods and the very pronounced trend during spring makes us consider that the trend during springtime reflects real changes in the atmosphere rather than drift in the instrument's sensitivity.

When compared to the cloud cover derived from the ERA5 reanalysis data the cloud cover for the winter (0.57 ± 0.003) is larger than the cloud cover for the summer (0.44 ± 0.002). For the cloud cover during spring the observed and ERA5 reanalysis data differ—the low cloud cover in the ceilometer observations (0.37 ± 0.005) is not found in the ERA5 reanalysis data (0.57 ± 0.004). In the latter the cloud cover falls nicely between the summer and winter cloud cover values. A significant reduction in the cloud cover during autumn 2016 is present in both the observed and ERA5 reanalysis data which prompted further investigations. It may have a relationship to the Pacific Decadal Oscillation or some other large scale oscillation.

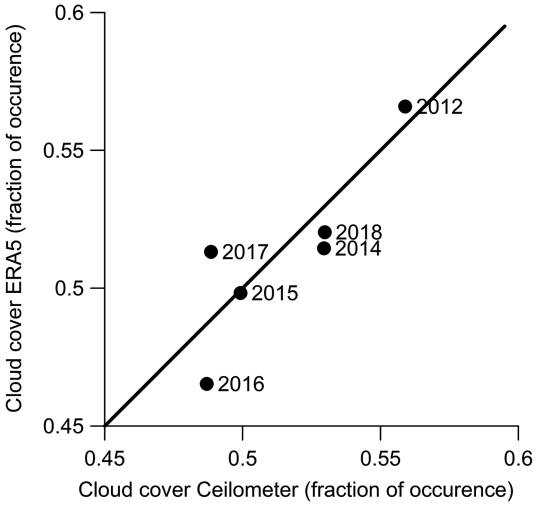

FIGURE 5 Scatter diagram of the annually averaged cloud cover derived from ceilometer measurements versus reanalysis data. Data from the years 2011 and 2013 are omitted due to large periods of missing observations

6 | PREDICTIVE SKILLS

6.1 | Theory

How well does the reanalysis data predict cloud cover? Because the distribution of the cloud cover is often U-shaped and thus does not resemble a Gaussian distribution, traditional methods for model evaluations should be used with caution and can even be misleading (Hogan *et al*., 2009). This has resulted in the use of applications that are based on skill scores (Mace *et al*., 1998; Miller *et al*., 1999; Palm *et al*., 2005; Wilkinson *et al*., 2008). These methods are based on expressing the number of joint occurrences of observed and predicted cloud cover that is greater or less than a prescribed threshold value in a contingency table. Traditionally a 2×2 contingency table is formed where the four joint occurrences reflect the number of (a) hits, (b) false alarms, (c) misses and (d) correct negatives (Table 3 and Figure 7).

Hogan *et al*. (2009) provides the relationship between the numbers of hits (a), false alarm (b), misses (c) and correct negatives (d) and the related numbers that would be obtained by a random prediction with the same

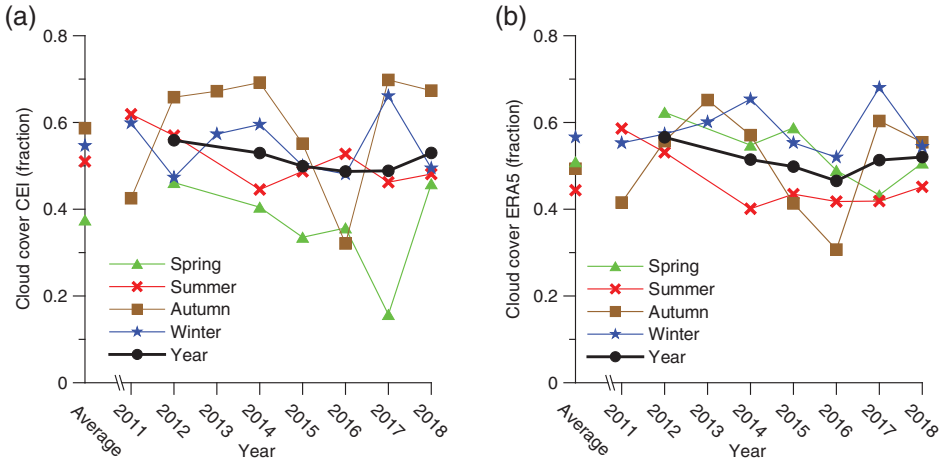

FIGURE 6 Seasonal and annual averaged cloud cover up to 6 km. (a) represents values derived from the ceilometer observations. The values in (b) are obtained from the reanalysis data (ERA5). The symbols on the left of each plot show the average skill score for the whole period for each of the seasons [Colour figure can be viewed at wileyonlinelibrary.com]

TABLE 3 A 2 × 2 contingency table of joint occurrence of cloud cover, where C_{mea} is observed cloud cover, C_{ERA5} is the predicted and C_{tr} is a cloud cover threshold

	$C_{mea} > C_{tr}$	$C_{mea} \leq C_{tr}$
$C_{ERA5} > C_{tr}$	Hits (cloud cover observed and predicted)	False alarm (cloud cover not observed but predicted)
$C_{ERA5} \leq C_{tr}$	Miss (cloud cover observed but not predicted)	Correct negative (cloud cover not observed or predicted)

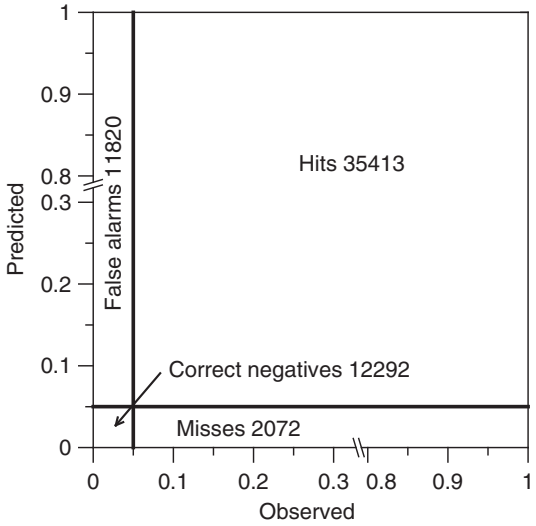

FIGURE 7 The 2 × 2 quadrant contingency table that is used for the skill score calculation for a cloud cover threshold value, C_{tr}, of 0.05. The hits, misses, false alarms and correct negatives are shown as well as the number of joint observations for the total period in each quadrant

statistical distribution of hits (a_r), false alarms (b_r), misses (c_r) and correct negatives (d_r), where

$$a_r = (a+b)(a+c)/n, \tag{5}$$

$$b_r = (a+b)(b+d)/n, \tag{6}$$

$$c_r = (c+d)(a+c)/n, \tag{7}$$

$$d_r = (c+d)(b+d)/n, \tag{8}$$

where $n = a + b + c + d$ is the total number of observations.

There exists a large number of statistical ways that can be used to derive a single number that reflects the quality of the comparison of the parameters in a contingency table—the numbers from the different methods are not consistent and therefore it is difficult to compare and the results should only be used in a relative sense. Hogan *et al.* (2009) reviewed the skill score methods with specific emphasis on their use in cloud cover comparisons. They pointed out that it is essential that the methods should be "equitable," which ensure that random predictions are assigned a score of zero, and in the case of perfect agreement a score of one.

Here we apply a generalized skill score (S) that fulfils the equitable requirement

$$S = \frac{x - x_r}{x_p - x_r}, \tag{9}$$

where x is a number that is derived from a function that reflects the agreement between the observed and modelled cloud cover, x_r is the value that would be obtained from a random prediction and x_p from a perfect prediction. It can be seen from Equation (9) that $S = 1$ for a perfect prediction and $S = 0$ for a prediction without any skill.

Heidke (1926) suggested a skill score by setting $x = a + d$, corresponding to the sum of hits and correct negatives, and consequently

$$x_r = a_r + d_r, \tag{10}$$

and the value corresponding to perfect prediction is $x_p = a + b + c + d$, corresponding to the total number of predictions. By inserting x_r and x_p in Equation (9) the Heidke skill score (HSS) can be written,

$$\mathrm{HSS} = \frac{2(ad - bc)}{(a+c)(c+d) + (a+b)(b+d)}. \tag{11}$$

The Heidke (1926) skill score applies a binary cloud/no-cloud discretization and does not take advantage of any detailed information that is available on the actual difference between predicted and observed cloud cover. A skill score that applied the mean-square error between predictions and observations was suggested by Murphy (1988) by setting the x-function in Equation (9) to be

$$x = \sum (\mathrm{pre} - \mathrm{obs})^2, \tag{12}$$

where pre is the predicted and obs the observed cloud cover. This skill score is abbreviated MSESS (mean squared error skill score). Along the same line Hogan *et al.* (2009) introduced the mean absolute error skill score (MAESS) by applying the x-function in Equation (9),

$$x = \sum |\mathrm{pre} - \mathrm{obs}|. \tag{13}$$

For both MSESS and MAESS, the random function, x_r , that should be used in Equation (9) is given in Equation (10) and the function representing perfect agreement is $x_p = 0$.

6.2 | Seasonal and annual skill scores

The seasonal and annual skill scores of the ability of the reanalysis to predict the observations of the cloud cover are illustrated in Figure 8. Qualitatively there is good agreement between the ranking by the HSS, MSESS and MAESS of the seasonal and annual cloud cover. A quantitative comparison between the methods is not possible as already pointed out earlier. To facilitate the

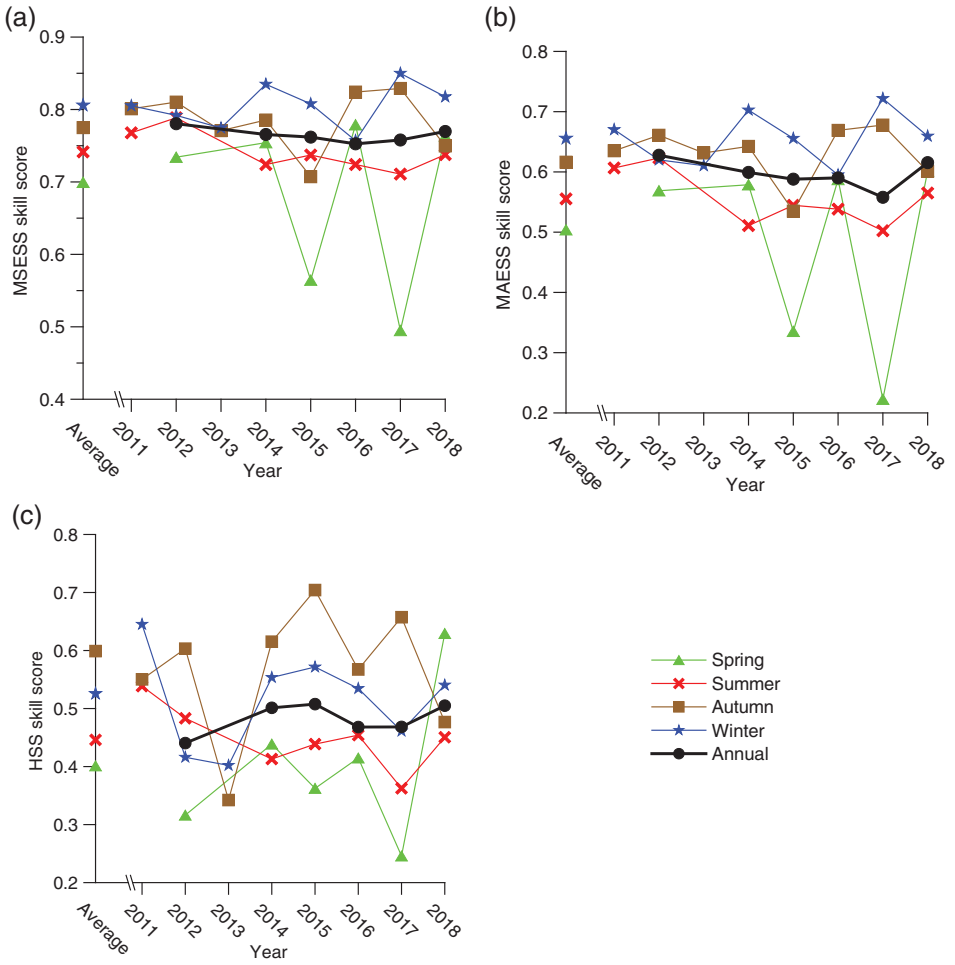

FIGURE 8 Seasonal and annual skill scores for MSESS (a), MAESS (b) and HSS (c) as a function of year. The symbols on the left of each plot shows the average skill score for the whole period for each of the seasons [Colour figure can be viewed at wileyonlinelibrary.com]

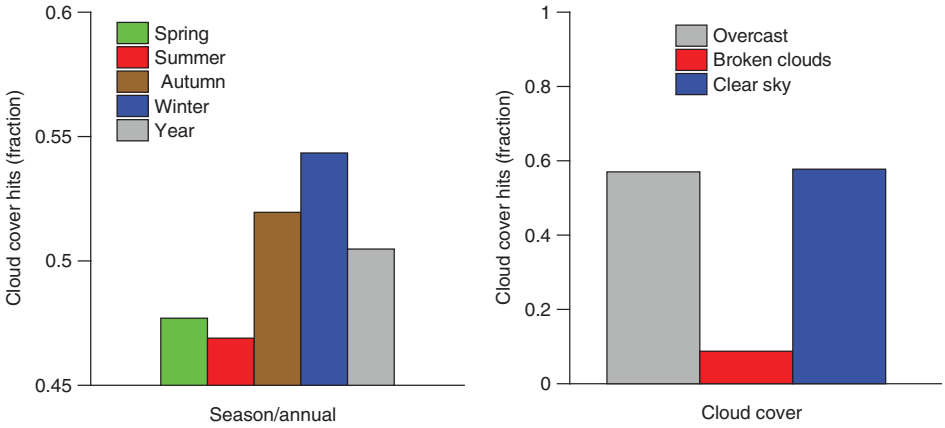

FIGURE 9 Hit statistics for a cloud cover resolution of 0.1. Left panel shows the result for the seasons when summing over all cloud cover data, and the right panel shows the cloud cover for the total period including all seasons [Colour figure can be viewed at wileyonlinelibrary.com]

comparison, the overall mean skill scores for the total period (2011–2019) are shown on the *y*-axis of Figure 8 as well. Generally, the prediction of the cloud cover during autumn and winter is better than for spring and summer. The prediction for the winter season is the best, except for HSS, and the spring season is always the poorest.

To investigate further the issue of cloud cover predictability, the fraction of hits for a joint histogram with a range separation for the cloud cover of 0.1 is shown in Figure 9. In agreement with the ranking by the skill scores, autumn and winter seasons have the better predictability (higher number of hits) as compared to spring and summer seasons. The winter season has the highest number of hits and the lowest is found for the summer season, the latter contrasts with the ranking by the skill scores. Figure 9 illustrates the hit statistics for overcast, broken cloud and clear sky conditions for a range resolution of 0.1 in the joint histogram, where overcast corresponds to a cloud cover range of 0.9–1.0, broken cloud to 0.1–0.9 and clear sky conditions corresponding to 0–0.1, respectively. The hit rate is ≈0.57 for both overcast and clear sky conditions, and much less, ≈0.09 for conditions of broken clouds.

7 | DISCUSSION

The Arctic amplification of climate warming is attributed to several factors where particular clouds are known to be a major contributor (Curry *et al.*, 1996; Boy *et al.*, 2019). However, the features and persistence of clouds are not well captured in numerical models, which contributes to the large spread among climate models (Karlsson and Svensson, 2011). The Arctic cloud seasonality is complex with different processes and atmospheric conditions operating in different temporal scales.

This has spurred interest in the cloud measurements in the Arctic but such measurements are very difficult due to the harsh conditions for the instruments. At the following sites, the results at the VRS are compared to extensive long time series of clouds that have been performed at

- Ny-Ålesund on the western coast of Svalbard in the Greenland Sea at the northern limit of the warm Gulf Stream (e.g., Maturilli and Ebell, 2018).
- On a ship frozen into the Arctic sea pack 570 km northeast of Prudhoe, Alaska in the yearlong SHEBA drift experiment (Intrieri *et al.*, 2002).
- The Eureka observatory (Shupe *et al.*, 2011), embedded within the Canadian archipelago.
- The Barrow observatory located on the northern coast of Alaska and its sister observatory Atqusuk located 100 km inland from Barrow.

Some overall features can be gleaned from Dong *et al.* (2010) and Shupe *et al.* (2011, figs 5 and 7). Common to these observations is the annual minimum in the cloud cover that typically varies from January to April. The minimum cloud cover is reported to occur at Ny-Ålesund, Barrow and Atqusuk in March, during the SHEBA experiment in January/February and at the Eureka observatory in May. This is in overall agreement with the observations at Station Nord (Figure 6) having a minimum in cloud cover during spring.

In late summer and autumn cloud occurrence generally is more frequent and with a less pronounced maximum as compared to the spring minimum. At Ny-Ålesund the maximum occurs in August, at Barrow in August–September (Dong *et al.*, 2010), at Eureka and SHEBA in September and at Atqusuk in October. Overall this is in agreement with the findings at Station Nord for a higher fraction of cloud cover during the autumn.

Therefore, the annual behaviour of the cloud cover in the high Arctic characterized with a minimum during the spring is also found at Station Nord followed by a high and fairly constant cloud cover with a less

pronounced maximum during autumn. The analysis of the cloud cover presented in Figure 6 shows that the annual variability of the seasonal cloud cover shows large variations between the years with no clear trend to be discerned, except for the cloud cover during spring, where a general decrease between 2012 and 2017 can be noticed.

Contrary to the observations by the ceilometer, reanalysis data does not show a smaller cloud cover during spring. The general decrease in the cloud cover during spring that was observed between 2012 and 2017 is also present in the reanalysis data, although the decrease is less pronounced. In both observed and reanalysis data there is a very distinct reduction of the cloud cover during the autumn of 2016. Both the disagreement on the cloud cover during spring and the agreement during the large reduction of cloud cover during the autumn of 2016 deserve further investigations.

Clouds display large backscattering which may vary by several orders of magnitude for different types of clouds. The choice of the threshold value for the attenuated backscatter coefficient is based on Vaughan (2002), who suggested a value of 1.4×10^{-5} sr^{-1} m^{-1} for cirrus clouds and several orders of magnitude larger for other types of clouds. An exception is polar stratospheric clouds, consisting mainly of ice particles, that were assigned a backscatter coefficient of 3×10^{-7} sr^{-1} m^{-1}. This value is near the detection limit of the ceilometer, but polar stratospheric clouds occur at heights beyond what can be reached by the ceilometer in its current configuration. In a study of clouds over Helsinki, Tuononen *et al*. (2019) applied a threshold value of 2×10^{-5} sr^{-1} m^{-1} in agreement with the recommendations in the Cloudnet approach by Illingworth *et al*. (2007). In order to investigate the sensitivity to the threshold value, the analysis in this study was carried out for a threshold value of 10^{-5} sr^{-1} m^{-1} as well as 2×10^{-5} sr^{-1} m^{-1}. It was found that the choice of threshold value did have a minor effect on the results and did not affect the overall conclusions in this manuscript.

In general the statistics of cloud cover estimated by an observer following the WMO standard (World Meteorological Organization, 2018) and from observations by a ceilometer on short time scales shows systematic deviations due to the fundamentally different approaches that are applied.

A cloud cover estimated by an observer represents a snapshot of the area averaged cloud cover divided into oktas. Total cloud cover (8/8) represents a fully cloud covered sky without any visible clear sky, and complementary (0/8) is a sky totally without any traces of clouds.

In contrast, observations by a ceilometer represent cloud cover divided into bins at a specific point in the sky, usually with the ceilometer pointing towards zenith or near-zenith, averaged over time. In this paper fully covered sky will fall within the range 0.9–1, and a clear sky 0.1–0, respectively. The two cloud cover approaches are therefore fundamentally different in several ways, including the way that full cloud cover and a clear sky are reported. As a consequence of the difference in the attribution of the cloud cover estimated by an observer will contain relatively fewer observations of 0/8 and 8/8 oktas whereas for a ceilometer there will be more observations in the corresponding bins, being 0–0.1 and 0.9–1, respectively.

While short-term cloud cover estimates will be different for the two methods, the two methods are expected to provide statistically near-similar results when averaged over longer times. Estimates of the cloud cover performed by an observer will inevitable have a subjective element, being in contrast to the fully objective and physical transparent ceilometer observations.

8 | CONCLUSIONS

Based on ceilometer observations and reanalysis data (ERA5) of the cloud fraction at Station Nord up to a height of 6 km during the period 2011–2019 it was found that

- The ceilometer worked well during the harsh conditions in the high Arctic.
- The observations of the cloud cover at Station Nord exhibit a minimum during spring and reach a maximum during the autumn; this is in overall agreement with variation of the cloud cover that is reported from other observatories in the high Arctic.
- The hourly averaged cloud cover follows a U-shaped distribution for both the observed and reanalysis data.
- The observed cloud cover for the individual seasons is rather erratic. A negative trend in the cloud cover between 2012 and 2017 is seen for spring and no clear trend is observed for the other seasons.
- The observed negative trend for the cloud cover during spring is less pronounced in the reanalysis data, and the low values of the observed cloud cover are not found in the reanalysis data.
- There is good agreement (correlation coefficient 0.86; root-mean-square error 0.016) between the annual averaged cloud cover from observations and reanalysis data.
- The predictive skill of the cloud cover of the reanalysis data was derived by three methods, all based on non-Gaussian joint statistics (MSESS, MAESS and Heidke). The skills in all the applied methods were found to be

better for the autumn and winter seasons and worse for the spring season.
- The hit rate (hourly clouds both observed and predicted in a joint histogram with a resolution of 0.1) is better for autumn and winter and worse for the summer season.
- The hit rates are near-equal for overcast and clear sky conditions and worse for broken sky conditions.

ACKNOWLEDGEMENTS

We acknowledge the project: Monitoring of short lived climate components in Arctic (in danish: "Monitering af kortlivede klimakomponenter i Arktis"). We thank the Danish Environmental agency for funding and the Villum Research Station for hosting the ceilometer. The study is also supported by National Science Fund of Bulgaria, Contract KP-06-N34/1 "Natural and anthropogenic factors of climate change – analyses of global and local periodical components and long-term forecasts." The work is related to activities of three of the authors (Sven-Erik Gryning, Ekaterina Batchvarova and Rogier Floors) within the COST Action CA18235 PROBE (PROfiling the atmospheric Boundary layer at European scale). We thank Paul Halton who kindly read through the manuscript.

ORCID

Sven-Erik Gryning https://orcid.org/0000-0001-5451-6510

REFERENCES

Boy, M., Thomson, E.S., Navarro, J.C.A., Arnalds, O., Batchvarova, E., Bäck, J., Berninger, F., Bilde, M., Dagsson-Waldhauserova, P., Castarède, D., Dalirian, M., De Leeuw, G., Dragosics, M., Duplissy, E.M., Duplissy, J., Ekman, A.M.L., Fang, K., Gallet, J. C., Glasius, M., Gryning, S.E., Grythe, H., Hansson, H.-C., Hansson, M., Isaksson, E., Iversen, T., Jonsdottir, I., Kasurinen, V., Kirkevåg, A., Korhola, A., Krejci, R., Kristjansson, J.E., Lappalainen, H.K., Lauri, A., Leppäranta, M., Lihavainen, H., Makkonen, R., Massling, A., Meinander, O., Nilsson, E.D., Olafsson, H., Pettersson, J.B.C., Prisle, N.L., Riipinen, I., Roldin, P., Ruppel, M., Salter, M., Sand, M., Seland, Ø., Seppä, H., Skov, H., Soares, J., Stohl, A., Ström, J., Svensson, J., Swietlicki, E., Tabakova, K., Thorsteinsson, T., Virkkula, A., Weyhenmeyer, G.A., Wu, Y., Zieger, P. and Kulmala, M. (2019) Interactions between the atmosphere, cryosphere, and ecosystems at northern high latitudes. *Atmospheric Chemistry and Physics*, 19(3), 2015–2061.

Chernokulsky, A. and Mokhov, I.I. (2012) Climatology of total cloudiness in the arctic: an intercomparison of observations and reanalyses. *Advances in Meteorology*, 2012, 16–18.

Curry, J.A., Rossow, W.B., Randall, D. and Schramm, J.L. (1996) Overview of arctic cloud and radiation characteristics. *Journal of Climate*, 9(8), 1731–1764.

Dong, X., Xi, B., Crosby, K., Long, C.N., Stone, R.S. and Shupe, M. D. (2010) A 10 year climatology of Arctic cloud fraction and radiative forcing at Barrow, Alaska. *Journal of Geophysical Research Atmospheres*, 115(17), D17212.

Esau, I. and Sorokina, S. (2011) Climatology of the arctic planetary boundary layer. In: Lang, P.R. and Lombargo, F.S. (Eds.) *Atmospheric Turbulence, Meteorological Modeling and Aerodynamics*. New York, NY: Nova Science.

Forbes, R. and Tompkins, A.M. (2011) An improved representation of cloud and precipitation. *ECMWF Newsletter*, 129(129), 13–18.

Forbes, R.M. and Ahlgrimm, M. (2014) On the representation of high-latitude boundary layer mixed-phase cloud in the ECMWF global model. *Monthly Weather Review*, 142(9), 3425–3445.

Forbes, R.M., Tompkins, A.M. and Untch, A. (2011) *A new prognostic bulk microphysics scheme for the ECMWF forecast model*. Reading: European Centre for Medium-Range Weather Forecasts. Technical memorandum 649.

Hahn, C.J., Warren, S.G. and London, J. (1995) The effect of moonlight on observation of cloud cover at night, and application to cloud climatology. *Journal of Climate*, 8(5), 1429–1446.

Heidke, P. (1926) Calculations of the success and goodness of strongwind forecasts in the storm warning service. *Geografiska Annaler Stockholm*, 8, 301–349.

Hersbach, H., Bell, B., Berrisford, P., Hirahara, S., Horányi, A., Muñoz-Sabater, J., Nicolas, J., Peubey, C., Radu, R., Schepers, D., Simmons, A., Soci, C., Abdalla, S., Abellan, X., Balsamo, G., Bechtold, P., Biavati, G., Bidlot, J., Bonavita, M., Chiara, G.D., Dahlgren, P., Dee, D., Diamantakis, M., Dragani, R., Flemming, J., Forbes, R., Fuentes, M., Geer, A., Haimberger, L., Healy, S., Hogan, R.J., Hólm, E., Janisková, M., Keeley, S., Laloyaux, P., Lopez, P., Lupu, C., Radnoti, G., Rosnay, P.D., Rozum, I., Vamborg, F., Villaume, S. and Thépaut, J.-N. (2020) The ERA5 global reanalysis. *Quarterly Journal of the Royal Meteorological Society*, 146, 1999–2049.

Hobbs, P.V. and Rangno, A.L. (1990) Rapid development of high ice particle concentrations in small polar maritime cumuliform clouds. *Journal of the Atmospheric Sciences*, 47(22), 2710–2722.

Hogan, R.J. and Illingworth, A.J. (2000) Deriving cloud overlap statistics from radar. *Quarterly Journal of the Royal Meteorological Society*, 126(569), 2903–2909.

Hogan, R.J., Jakob, C. and Illingworth, A.J. (2001) Comparison of ECMWF winter-season cloud fraction with radar-derived values. *Journal of Applied Meteorology*, 40(3), 513–525.

Hogan, R.J., O'Connor, E.J. and Illingworth, A.J. (2009) Verification of cloud-fraction forecasts. *Quarterly Journal of the Royal Meteorological Society*, 135(643), 1494–1511.

Illingworth, A.J., Hogan, R.J., O'Connor, E.J., Bouniol, D., Brooks, M.E., Delanoé, J., Donovan, D.P., Eastment, J.D., Gaussiat, N., Goddard, J.W.F., Haeffelin, M., Baltink, H.K., Krasnov, O.A., Pelon, J., Piriou, J.-M., Protat, A., Russchenberg, H.W.J., Seifert, A., Tompkins, A.M., van Zadelhoff, G.-J., Vinit, F., Willen, U., Wilson, D.R. and Wrenc, C.L. (2007) CLOUDNET continuous evaluation of cloud profiles in seven operational models using ground-based observations. *Bulletin of the American Meteorological Society*, 88(6), 883–898.

Intrieri, J.M., Shupe, M.D., Uttal, T. and McCarty, B.J. (2002) An annual cycle of Arctic cloud characteristics observed by radar

and lidar at SHEBA. *Journal of Geophysical Research: Oceans*, 107(10), 8030.

Karlsson, J. and Svensson, G. (2011) The simulation of Arctic clouds and their influence on the winter surface temperature in present-day climate in the CMIP3 multi-model dataset. *Climate Dynamics*, 36, 623–635.

Key, J. and Barry, R.G. (1989) Cloud cover analysis with Arctic AVHRR data: 1. Cloud detection. *Journal of Geophysical Research*, 94(D15), 18521.

Mace, G.G. and Benson-Troth, S. (2002) Cloud-layer overlap characteristics derived from long-term cloud radar data. *Journal of Climate*, 15(17), 2505–2515.

Mace, G.G., Jakob, C. and Moran, K.P. (1998) Validation of hydrometeor occurrence predicted by the ECMWF model using millimeter wave radar data. *Geophysical Research Letters*, 25(10), 1645–1648.

Maturilli, M. and Ebell, K. (2018) Twenty-five years of cloud base height measurements by ceilometer in Ny-Ålesund, Svalbard. *Earth System Science Data*, 10(3), 1451–1456.

McFarquhar, G.M., Zhang, G., Poellot, M.R., Kok, G.L., McCoy, R., Tooman, T., Fridlind, A. and Heymsfield, A.J. (2007) Ice properties of single-layer stratocumulus during the mixed-phase Arctic cloud experiment: 1. Observations. *Journal of Geophysical Research*, 112(D24), D24201.

Miller, S.D., Stephens, G.L. and Beljaars, A.C.M. (1999) A validation survey of the ECMWF prognostic cloud scheme using LITE. *Geophysical Research Letters*, 26(10), 1417–1420.

Murphy, A.H. (1988) Skill scores based on the mean square error and their relationships to the correlation coefficient. *Monthly Weather Review*, 116(12), 2417–2424.

Palm, S.P., Benedetti, A. and Spinhirne, J. (2005) Validation of ECMWF global forecast model parameters using GLAS atmospheric channel measurements. *Geophysical Research Letters*, 32(22), L22S09.

Pinto, J.O. (1998) Autumnal mixed-phase cloudy boundary layers in the Arctic. *Journal of the Atmospheric Sciences*, 55(11), 2016–2038.

Platt, C.M., Young, S.A., Carswell, A.I., Pal, S.R., McCormick, M.P., Winker, D.M., Delguasta, M., Stefanutti, L., Eberhard, W.L., Hardesty, M., Flamant, P.H., Valentin, R., Forgan, B., Gimmestad, G.G., Jäger, H., Khmelevtsov, S.S., Kolev, I., Kaprieolev, B., Lu, D.-R., Sassen, K., Shamanaev, V.S., Uchino, O., Mizuno, Y., Wandinger, U., Weitkamp, C., Ansmann, A. and Wooldridge, C. (1994) The Experimental Cloud Lidar Pilot Study (ECLIPS) for cloud-radiation research. *Bulletin of the American Meteorological Society*, 75(9), 1635–1654.

Rau, G. and Piringer, M. (2018) Dispersion categories from visual observations compared to those derived by a ceilometer system and satellite cloud cover information. *Meteorologische Zeitschrift*, 27(3), 209–221.

Rossow, W.B. (1993) Satellite observations of radiation and clouds to diagnose energy exchanges in the climate: part II. In: *Energy and Water Cycles in the Climate System*. Berlin-Heidelberg: Springer, pp. 143–164.

Shupe, M.D., Walden, V.P., Eloranta, E., Uttal, T., Campbell, J.R., Starkweather, S.M. and Shiobara, M. (2011) Clouds at Arctic atmospheric observatories. Part I: occurrence and macrophysical properties. *Journal of Applied Meteorology and Climatology*, 50(3), 626–644.

Skov, H., Bossi, R., Christensen, J., Vorkamp, K., Massling, A., Nøjgaard, J.K., Hansen, K.J., Im, U. and Sørensen, L.L. (2020) *The importance of the Villum Reserach Station for the Danish atmospheric AMAP contributions*. Aarhus: Aarhus University, DCE – Danish Centre for Environment and Energy. Technical report number: 165, 26 pp. Available at: http://dce2.au.dk/pub/TR165.pdf [Accessed 21st October 2020].

Skov, H., Massling, A.H., Nielsen, I.E., Nordstrøm, C., Bossi, E., Vorkamp, K., Christensen, J., Larsen, M.M., Hansen, K.M., Liisberg, J.B. and Poulsen, M.B. (2017) *AMAP core: atmospheric part*. Aarhus: Aarhus University, DCE – Danish Centre for Environment and Energy. Technical report number: 101. Available at: https://dce2.au.dk/pub/TR101.pdf [Accessed 21st October 2020].

Suomi, I., Lüpkes, C., Hartmann, J., Vihma, T., Gryning, S.-E. and Fortelius, C. (2016) Gust factor based on research aircraft measurements: a new methodology applied to the Arctic marine boundary layer. *Quarterly Journal of the Royal Meteorological Society*, 142(701), 2985–3000.

Tompkins, A.M. and Di Giuseppe, F. (2015) An interpretation of cloud overlap statistics. *Journal of the Atmospheric Sciences*, 72 (8), 2877–2889.

Tuononen, M., O'Connor, E.J. and Sinclair, V.A. (2019) Evaluating solar radiation forecast uncertainty. *Atmospheric Chemistry and Physics*, 19(3), 1985–2000.

Uttal, T., Makshtas, A. and Laurila, T. (2013) The Tiksi international hydrometeorological observatory. *WMO Bulletin*, 62(1), 22–26.

Vande Hey, J.D. (2015) *A Novel Lidar Ceilometer*. Cham: Springer International, 158 pp.

Vaughan, J.M. (2002) Scattering in the atmosphere. In: Pike, R. and Sabatier, P. (Eds.) *Scattering*. Amsterdam: Elsevier, pp. 937–957.

Wilkinson, J.M., Hogan, R.J., Illingworth, A.J. and Benedetti, A. (2008) Use of a Lidar Forward Model for global comparisons of cloud fraction between the ICESat Lidar and the ECMWF model. *Monthly Weather Review*, 136(10), 3742–3759.

World Meteorological Organization. (2018) Observation of clouds. In: *WMO Guide to Meteorological Instruments and Methods of Observations (the CIMO Guide)*, 2017th edition. Geneva: World Meteorological Organization. Available at: https://www.wmo.int/pages/prog/www/IMOP/CIMO-Guide.html [Accessed 21st October 2020].

How to cite this article: Gryning S-E, Batchvarova E, Floors R, Münkel C, Skov H, Sørensen LL. Observed and modelled cloud cover up to 6 km height at Station Nord in the high Arctic. *Int J Climatol*. 2021;41:1584–1598. https://doi.org/10.1002/joc.6894